

Full Length Article

Novel green chemical mechanical polishing of fused silica through designing synergistic CeO₂/h-BN abrasives with lubricity

Jie Liu ^a, Zhenyu Zhang ^{a,*}, Chunjing Shi ^{b,*}, Zheng Ren ^c, Junyuan Feng ^a, Hongxiu Zhou ^d, Zhensong Liu ^a, Fanning Meng ^b, Shuming Zhao ^c

^a State Key Laboratory of High-performance Precision Manufacturing, Dalian University of Technology, Dalian 116024, China

^b School of Mechanical Engineering, Hangzhou Dianzi University, Hangzhou 310018, China

^c China Academy of Ordnance Science Ningbo Branch, Ningbo 315103, China

^d School of Energy and Power Engineering, Dalian University of Technology, Dalian 116024, China

ARTICLE INFO

Keywords:

Fused silica
Chemical mechanical polishing
CeO₂
h-BN
Potassium oleate

ABSTRACT

It is a challenge to produce an atomic-scale surface of fused silica with a high material removal rate (MRR) using green chemical mechanical polishing (CMP). In traditional CMP, a slurry usually contains four or more components and is normally toxic and corrosive, causing environmental degradation. To address this problem, a novel green CMP slurry for fused silica was developed using ceria/hexagonal boron nitride (CeO₂/h-BN) abrasives, potassium oleate, and deionized water. Due to the two-dimensional nanosheet structure of h-BN, it is simple to generate a sheared layer, which lowers friction at the contact area. Ceria abrasives realized a new function for superlubricity during CMP through this design, preventing damages and reaching atomic-scale surface. This is confirmed by research showing that a damaged layer's thickness following CMP, as determined by high-resolution transmission electron microscopy, is only 2.7 nm. The MRR of fused silica is 31.92 $\mu\text{m}\cdot\text{h}^{-1}$ during CMP, and surface roughness Sa is 0.124 nm after CMP. The MRR is currently at its highest with such a low surface roughness. These findings provide a new pathway to achieve an atomic-scale surface for a hard-brITTLE material with a high MRR using the synergistic effect of abrasives.

1. Introduction

Fused silica (FS) is the material of choice for many high-performance optical elements due to its unmatched optical qualities and outstanding chemical, thermal, and radiation resistance [1–4]. Unfortunately, high-precision machining and manufacture of FS have been constrained by its hard and brittle nature [5,6]. The efficient preparation of FS optical surfaces with ultra-high surface quality in optical production remains a difficult task at the moment. Chemical mechanical polishing (CMP) technology [7–10] has been applied to the treatment of FS and great progress has been made to meet the high surface quality requirements of FS.

The two main components of CMP technology are chemical corrosion and mechanical removal [11]. In light of this, the polishing slurry—which offers the potential for chemical reaction and grinding force—has drawn considerable interest in a variety of polishing fields. The polishing slurry is one of the key elements impacting surface roughness and material removal rate (MRR) and is typically composed

of abrasives and chemical additives [12,13]. Due to its unique chemical characteristics, cerium oxide (CeO₂) can produce a greater MRR than silica (SiO₂) when used as an abrasive in polishing slurry. As such, CeO₂-based slurries have been extensively used in the CMP for silica. For instance, Zhang et al. [14] developed a CeO₂-based slurry containing ceria powder, oxalic acid, and deionized water (DIW) to polish silica glass, and the ideal MRR was 23.34 $\mu\text{m}\cdot\text{h}^{-1}$. However, within a measurement area of $10 \times 10 \mu\text{m}^2$, the completed surface's surface roughness was only 1.440 nm. The primary cause of this poor surface quality was the surface scratch brought on by the uneven morphology and aggregation of CeO₂. When the most popular kind of calcined CeO₂ was used as the abrasive in a single abrasive slurry, the surface scratch was particularly prevalent [15,16]. Many researchers, including Xu [7], Janos [17], Wu [18] and Kim [19], have tried to prepare CeO₂ abrasives with uniform morphology and superior polishing capabilities, and then apply them to the polishing slurry for silica glass, to solve the aforementioned problem. Although these techniques can improve surface quality and MRR, it is too difficult to control CeO₂'s form, size, and

* Corresponding authors.

E-mail addresses: zzy@dlut.edu.cn (Z. Zhang), shicj@hdu.edu.cn (C. Shi).

purity for commercial usage [20,21]. Therefore, at the moment, minimizing polishing scratch and enhancing surface quality are still long-term problems.

From a different angle, a technique that can alter the abrasives' direct mechanical impact on the workpiece and boost the lubrication between them might be useful for enhancing surface quality. Due to interlayer sliding and low shear stresses, most two-dimensional (2D) nanomaterials display superlubricity [22]. Because of their nanostructure, they may also enter the contact surface with ease and produce a lubricating coating that can smooth down rough edges and repair wear caused by abrasives. In general, promising lubricating materials include graphene [22], molybdenum disulfide (MoS_2) [23], MXene [24], and hexagonal boron nitride (h-BN) [23]. In particular, h-BN is a viable option due to its many advantages, including structural stability, chemical stability, and relatively low hardness (2 on the Mohs scale), as well as its affordability and environmental friendliness [25]. Therefore, h-BN has the potential to be used as an auxiliary abrasive in CMP slurries to improve lubricity and protect the sample surface from excessive wear.

Chemical additives in the polishing slurry help to produce a softer reaction layer on the sample surface, which is easily removed by the mechanical action of the abrasives [26]. To prevent irreparable damage to the users, the machinery, and the environment, green manufacturing principles should be used to guide the selection of the chemicals added to polishing slurries. The development of a CMP slurry for FS with a straightforward composition, great polishing performance, and no possible danger to people or the environment, however, has received little attention.

In this work, a novel CMP slurry for polishing FS was developed using CeO_2 nanoparticles, h-BN nanoflakes, potassium oleate (KOL), and DIW. The MRR and surface quality after polishing was greatly enhanced with the aid of the novel slurry. Optical microscopy, a non-contact three-dimensional (3D) optical surface profiler, and an atomic force microscope (AFM) were all employed simultaneously to observe the surface topography and roughness. High-resolution transmission electron microscopy (HRTEM) measurements and analyses were performed on the subsurface damage features of FS before and after CMP. Based on the examination of X-ray photoelectron spectroscopy (XPS) and Fourier transform infrared (FTIR) spectra, a functional mechanism for polishing FS with the developed slurry was provided.

2. Experimental details

2.1. Materials

FS (Lianyungang Julin Quartz Technology Co., Ltd., China) with a purity of more than 99.99% and a dimension of $10 \times 10 \times 5 \text{ mm}^3$ was used as the sample. We bought SiO_2 nanopowder with a mean size of about 300 nm from China's Bisili New Materials (Suzhou) Co., Ltd. Commercial calcined CeO_2 nanopowder with a mean size of $\sim 50 \text{ nm}$ was received from Xuancheng Jingrui New Materials Co., Ltd., China. h-BN nanoflake was obtained from Qinghe Kegong Metallurgical Materials Co., Ltd., China. Anhydrous ethanol and sodium hydroxide (NaOH) were bought from Shanghai Macklin Biochemical Technology Co., Ltd. in China. Polyethylene glycol 400 (PEG 400) was provided by Sinopharm Chemical Reagent Co., Ltd., China. KOL powder with a purity of more than 98% was obtained from Xiya Chemical Reagent Co., Ltd., China. Polyurethane and nubuck leather pads used in the experiments were both supplied by Shenyang Kejing Auto-instrument Co., Ltd., China. DIW was used throughout all the experiments, and the above reagents were of analytical grade and used directly without further treatment. All experiments were performed using a precision lapping/polishing machine (UNIPOL-1502, Shenyang Kejing Auto-instrument Co., Ltd., China).

2.2. Methods

In this work, FS was processed using sequential lapping and CMP. Additionally, each experiment was preceded by a minimum of 10 min of ultrasonically cleaning all samples in an anhydrous ethanol bath.

A high MRR is needed since the primary goals of lapping are to swiftly eliminate surface imperfections and provide a surface with a high degree of flatness. SiO_2 can remove a significant amount of material from FS without causing further harm because it has the same hardness as FS. SiO_2 was therefore chosen as the lapping abrasive. To increase the flowability and dispersibility of SiO_2 abrasives in the lapping slurry, PEG 400 was utilized as a liquid lubricant and dispersant. The optimum lapping slurry consisted of 5.0 wt% SiO_2 , 0.4 wt% PEG 400 and DIW. The two types of pads that are most frequently used for processing FS are polyurethane and nubuck leather. One of them, the polyurethane pad, has a higher hardness and is less prone to deformation while in use, which may make it easier to transfer slurry and increase the uniformity and processing efficiency of surface materials. As a result, a polyurethane pad was employed as the lapping pad, and process parameters including the rotational speed of the lapping disk, the lapping pressure, the flow rate of the lapping slurry, and the lapping duration were set, respectively, at 100 rpm, 35.2 kPa, $11.5 \text{ mL}\cdot\text{min}^{-1}$, and 30 min.

Four CMP slurries were first created, as shown in Table 1, and their polishing abilities were subsequently tested and examined. These slurries contained an abrasive made from commercially available calcined CeO_2 . To create an alkaline polishing environment, NaOH was used in slurry S1 as a pH regulator and KOL was added to the other slurries. All these slurries have the same alkalinity of ~ 10 . The nubuck leather pad's surface is porous and fluffy and has a lower hardness, which makes it easier to charge and discharge the slurry and obtain a high level of surface quality. Because of this, a nubuck leather pad was utilized in the CMP process, and the ideal process parameters, including the polishing disk speed, polishing pressure, CMP slurry feed rate, and polishing time, were set at 100 rpm, 35.2 kPa, $11 \text{ mL}\cdot\text{min}^{-1}$, and 45 min. The sample was ultrasonically washed with DIW and absolute ethanol for 10 min to remove residues after each polishing, and then it was dried with compressed gas. To avoid the deposition of abrasives, the lapping, and CMP slurries were mechanically swirled continuously during the experiment.

2.3. Characterization

The surface morphologies and sizes of CeO_2 and h-BN were observed by SEM (Quanta 200 FEG, FEI, USA) and TEM (JEM-1400Flash, JEOL, Japan). The sessile drop method [27,28] was used to determine the contact angles of the four CMP slurries on the surface of FS, and a drop shape analyzer (DSA100, KRUESS Scientific, Germany) was used to measure the drop shapes. The contact angle was determined by using Advance software to analyze the droplet shape, and the measurement result was the average of three repeated tests.

The microstructure of the FS sample was observed using an optical microscope (BX53M, Olympus, Japan). Accordingly, the 3D surface profile and roughness were described and measured using an AFM (JPK Nanowizard 4XP, Bruker, Germany) and a 3D optical surface profiler (NewView 9000, Zyglo, USA). The average value of surface roughness S_a at five randomly chosen sites was used as the measurement result to reduce measurement error. The 3D surface profiles recorded by the 3D optical surface profiler and AFM and displayed in this paper depict the

Table 1
Composition of CMP slurry.

CMP slurry	Composition	pH
S1	4.0 wt% CeO_2 + NaOH + DIW	~ 10
S2	4.0 wt% CeO_2 + 0.2 wt% KOL + 0.2 wt% h-BN + DIW	~ 10
S3	4.0 wt% CeO_2 + 0.2 wt% KOL + 0.4 wt% h-BN + DIW	~ 10
S4	4.0 wt% CeO_2 + 0.2 wt% KOL + 0.6 wt% h-BN + DIW	~ 10

ideal surface morphology, it should be stressed. The cross-sectional specimen of the FS sample was first prepared using focused ion beam (FIB) technology, and then studied by HRTEM (Talos F200X, Thermo Fisher Scientific, USA) to investigate the distribution of subsurface damage of FS before and after polishing. The MRR ($\mu\text{m}\cdot\text{h}^{-1}$) of the FS sample, which is obtained from the mass loss of the sample before and after each CMP, can be determined from Eq. (1).

$$\text{MRR} = \frac{60 \times \Delta m}{\rho \cdot S \cdot t} \times 10^4 \quad (1)$$

where Δm (g) is the mass loss of FS sample during CMP, the sample mass was weighed on a high precision electronic analytical balance (FA124, Shanghai Lichen Instrument Technology Co., Ltd., China) with a resolution of 0.1 mg, ρ is the density of FS sample with a value of $2.2 \text{ g}\cdot\text{cm}^{-3}$, S (cm^2) is polishing contact area, and t (min) is polishing time.

Both the elemental composition on the surface of FS and the valence states of particular elements in the CMP slurry were examined using XPS (Thermo Scientific ESCALab Xi+, Thermo Fisher Scientific, USA). Monochromatic Al K α radiation with an energy of 1486.6 eV was used as the X-ray source. All XPS spectra were analyzed using Thermo Avantage software, and all binding energies were corrected by the C 1 s signal at 284.8 eV [29,30] before analysis. The vibrational peaks of FS, KOL, and FS treated with various compounds were also investigated using the FTIR spectrometer (Thermo Scientific Nicolet iS20, Thermo Fisher Scientific, USA). Potassium bromide was used as a carrier for the infrared sample. The wavenumber range of each FTIR spectrum was 400–4000 cm^{-1} , and the spectral resolution was 4 cm^{-1} .

3. Results and discussion

3.1. Lapping treatment

Fig. 1 displays the 2D optical morphologies and 3D surface profiles of FS before and after lapping. The raw surface of FS had several defects, including scratches, pits, and other surface irregularities, as shown in **Fig. 1(a)**, and as shown in **Fig. 1(b)**, the surface roughness S_a was 64.990 nm with a measurement area of $100 \times 100 \mu\text{m}^2$. Only a few scratches

and pits remained after 30 min of lapping the raw surface with the lapping slurry (**Fig. 1(c)**). The majority of the imperfections had been eliminated, and the S_a was decreased to $\sim 1.255 \text{ nm}$ after lapping, as shown in **Fig. 1(d)**. In general, the significant improvement in surface finish following lapping may contribute to increased polishing process effectiveness.

3.2. Characterization of CMP slurry

The size and morphology of the abrasives used in the CMP slurry have been shown to significantly affect the polishing effect [31], therefore the morphological properties of the CeO₂ and h-BN utilized in this study were examined by SEM and TEM, as shown in **Fig. 2**. It can be observed from **Fig. 2(a)** and (b) that the CeO₂ nanoparticles have irregular shapes with sharp edges and corners. Additionally, the particle size ranged from 45 to 57 nm, with an average size of $50.48 \pm 2.33 \text{ nm}$, as shown by the diameter distribution of CeO₂ in **Fig. 2(c)**. CeO₂ can moderately wear FS since it has a little lower hardness than FS [32]. In addition, the chemical nature of CeO₂ makes it possible to react with FS. As a result, CeO₂ is physically and chemically unique, making it notably superior to other abrasives at polishing FS. **Fig. 2(d)** and (e) show that h-BN has a layered structure in the form of a nanosheet similar to graphite. It also shared graphene's crystal structure (**Fig. 2(f)**), often known as "white graphene" [33,34]. Each layer in the h-BN crystal structure is made up of boron and nitrogen atoms that are covalently linked, and these layers are held together by weak van der Waals forces [35].

On the surface of FS, the contact angles of the slurries indicated in **Table 1** were measured as shown in **Fig. 3(a)**. The wetting performance of the liquid is generally better the smaller the contact angle [36]. Lower contact angles were observed in slurries S2–S4 containing KOL as compared to slurry S1, suggesting that KOL can enhance slurry wettability while lowering contact angles. The most likely reason for this is that KOL, which possesses a hydrophilic head (carboxyl group in **Fig. 3(b)**), is an anionic surfactant. Due to its unique structure, it has a stronger affinity for water, which may help to reduce the slurry's surface tension and produce a stable suspension.

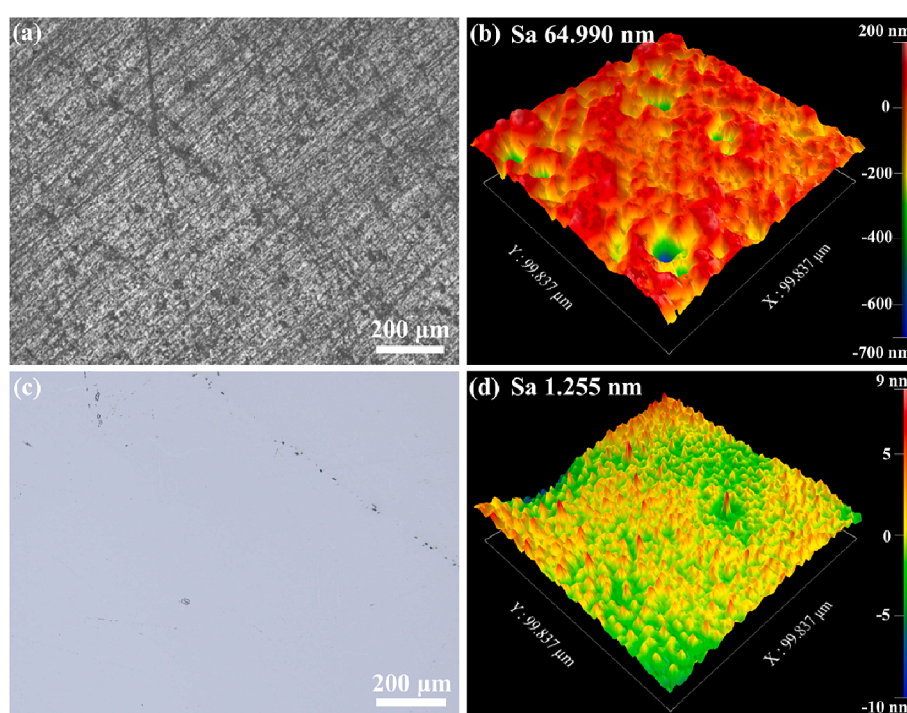


Fig. 1. Typical optical images and 3D morphologies of FS (a, b) before and (c, d) after lapping.

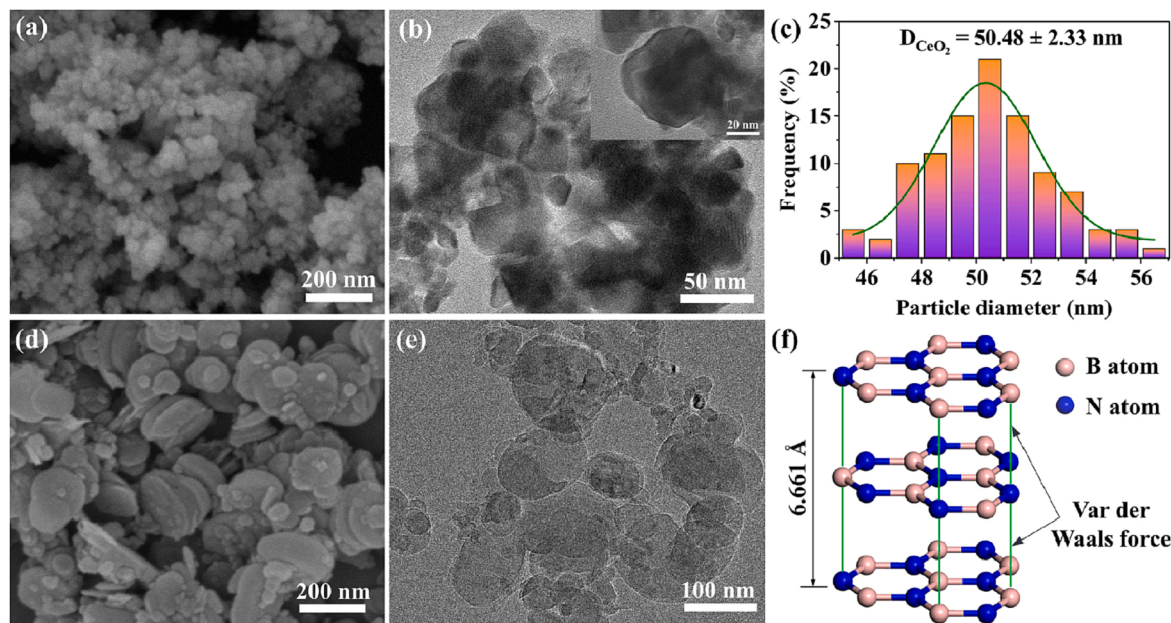


Fig. 2. (a) SEM, (b) TEM images, and (c) diameter distribution of CeO_2 , and (d) SEM, (e) TEM images, and (f) crystal structure of h-BN.

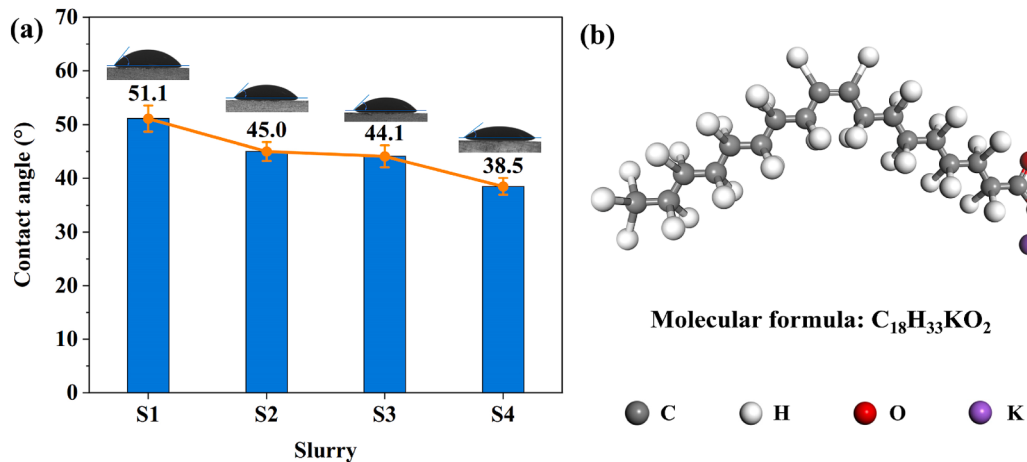


Fig. 3. (a) Contact angles of slurries and (b) the molecular structure of KOL.

3.3. Verification of CMP processing of FS

The schematic representation of the CMP process for FS is shown in Fig. 4, and it is based on the description in the methods section.

Additionally, as shown in Fig. 5, the polishing impact of slurries S1–S4 on FS, including the Sa and MRR, was examined. The Sa following polishing with slurries containing h-BN nanoflakes was considerably lower than that following polishing with slurries devoid of h-BN

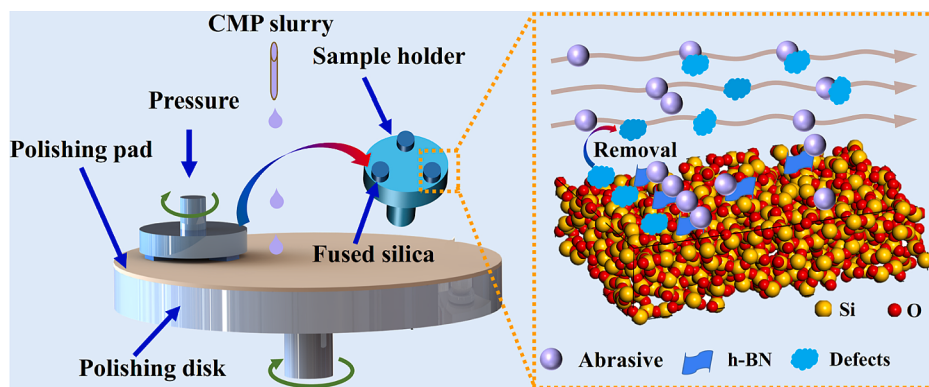


Fig. 4. Schematic illustration of CMP process for FS.

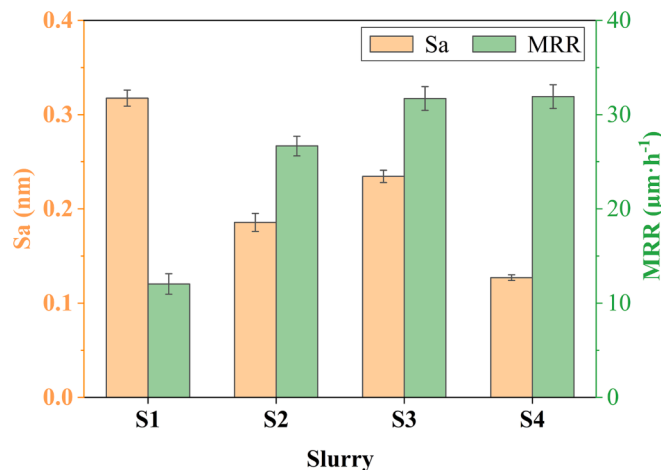


Fig. 5. Sa and MRR after CMP with slurries S1–S4.

nanoflakes. In other words, the surface quality was improved by the inclusion of h-BN nanoflakes as opposed to the slurry's single abrasive CeO₂. There are two potential explanations for this. First, the irregular morphology of CeO₂ nanoparticles in slurry S1 with a single type of abrasive could produce few surface defects including cracks, small scratches, etc., leading to a higher surface roughness. Second, because of the excellent lubricity of h-BN, some of them could serve as a solid lubricant between abrasives and the surface of FS as well as between abrasives and a polishing pad, reducing friction between them. This effect can convert the majority of CeO₂ abrasives' rolling motion from sliding to rolling, preventing excessive wear on the surface of the FS and resulting in a better finished surface.

Additionally, the MRR is inversely linked with the contact angle, as shown by Fig. 3(a) and 5. In other words, a small contact angle led to a higher MRR, whereas a large contact angle led to a lower MRR. The

effective slurry for polishing in slurry S1 was the lowest and the chemical activity was the weakest in the same alkaline polishing environment, resulting in a thinner surface modified layer on the surface of FS. Due to the similar hardness of the abrasive and the substrate, it is challenging to remove the substrate material once the thin modified layer has been removed with CeO₂ abrasives. In this case, the thinner modified layer resulted in a lower MRR. But by including KOL in the slurry, more slurry was able to effectively engage in the polishing procedure, allowing more material to react with the slurry and producing a thicker modified layer on the surface of the FS. The thick modified layer could be easily removed with CeO₂ abrasives in time, especially for slurry S4. Thus, slurry S4 produced the highest MRR. Slurry S4 had the best polishing effect overall among the four slurries, with the lowest Sa and maximum MRR. Therefore, the optimum composition of CMP slurry (called novel CMP slurry) for FS was 4.0 wt% CeO₂, 0.6 wt% h-BN, 0.2 wt% KOL and DIW.

The optical micrograph of FS after polishing with the novel CMP slurry is displayed in Fig. 6(a). The surface shows a smooth and flat surface without defects. The average value of Sa measured by the 3D optical surface profiler was 0.127 ± 0.003 nm, and the lowest value of Sa was 0.124 nm with a measurement area of $20 \times 20 \mu\text{m}^2$ (Fig. 6(b)), showing an ultra-low surface roughness. AFM was also used to characterize the surface profile of the corresponding sample, as illustrated in Fig. 6(c) and (d). The Sa measured by AFM was 0.125 nm with a measurement area of $10 \times 10 \mu\text{m}^2$, which is close to 0.124 nm measured by the 3D optical surface profiler. In conclusion, the flaws in Fig. 1(c) that persisted on the surface after lapping were eliminated, and the Sa was greatly decreased, following polishing FS using the novel CMP slurry. Additionally, the MRR estimated by Eq. (1) reached a maximum of $31.92 \mu\text{m}\cdot\text{h}^{-1}$. So far, the polishing results achieved here with such low roughness and ultra-high MRR are the best compared to previous reports [7,11,15,32,37–40].

Fig. 7 displays the subsurface damage characteristics of the FS before and after CMP with the novel CMP slurry. Specifically, the surface before CMP possessed a damaged layer (DL) with a depth of ~ 60.1 nm (Fig. 7

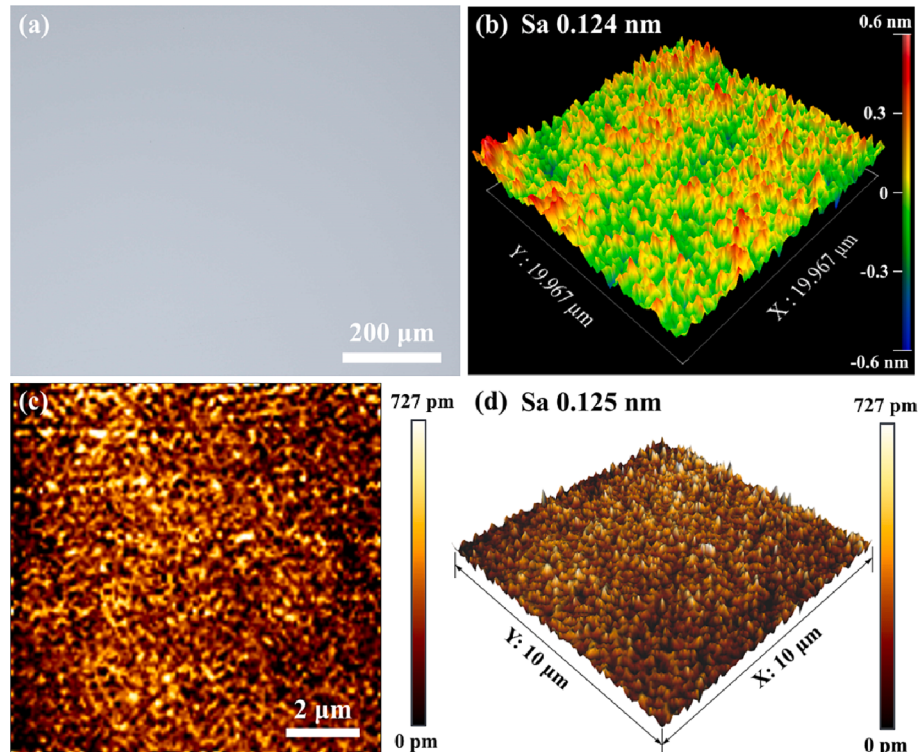


Fig. 6. (a) Optical micrograph, (b) 3D morphology measured by 3D optical surface profiler, (c) 2D and (d) 3D surface profiles measured by AFM of the polished surface with novel CMP slurry.

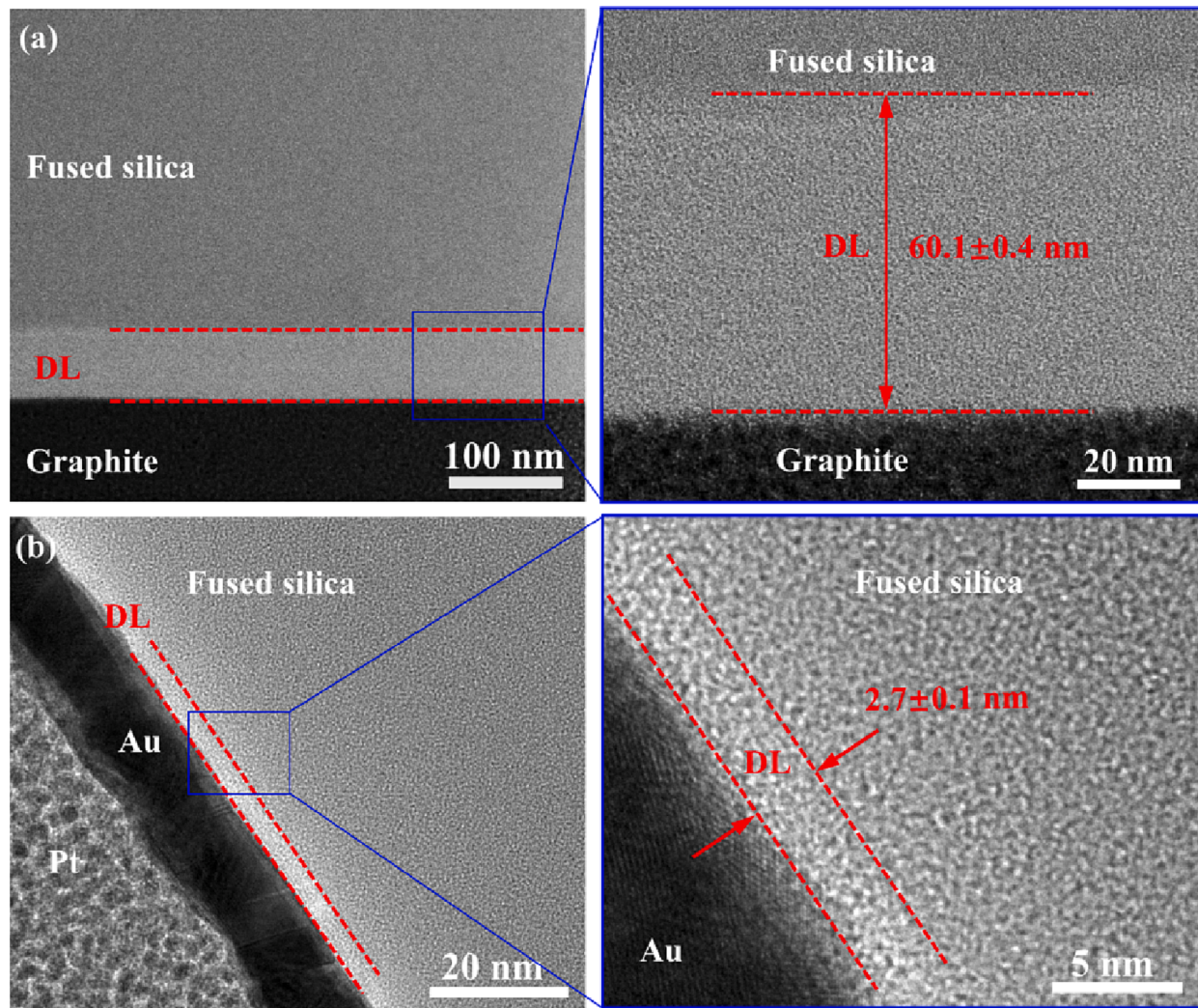


Fig. 7. Subsurface damage characteristic of FS (a) before and (b) after polishing with the novel CMP slurry.

(a)). The compressive stress of SiO_2 abrasives acting on the surface of FS during lapping may be the cause of such a deep DL. Lapping is a type of mechanical machining. During this process, the abrasives cause cutting and extrusion effects on the workpiece surface, resulting in plastic deformation of the surface material of the FS and ultimately the formation of a mechanical stress-induced DL. The mechanical stress-induced DL was interestingly almost completely removed following CMP, and no further flaws like surface cracks were created. Only a dense structure with a depth of ~ 2.7 nm remained, as shown in Fig. 7(b). The thin DL shows that there was no brittle fracture removal during the CMP procedure. The aforementioned results show that a high-quality surface with extremely little damage was created by combining the novel CMP slurry with the CMP methods described in this paper.

3.4. Analysis of the CMP mechanism of FS

To explore the CMP mechanism of FS, the valence states of specific elements in the CMP slurry before and after cyclic polishing were measured by XPS. Fig. 8(a)–(c) describe the XPS characteristic spectra of the fresh slurry. In Fig. 8(a), the fresh slurry's O 1 s spectra show two major peaks at 529.13 and 531.47 eV, which are caused by the O^{2-} species in Ce^{4+} and Ce^{3+} , respectively [7]. The thermodynamic instability of CeO_2 in the aqueous environment, which caused some Ce elements to be reduced from Ce^{4+} to Ce^{3+} , is primarily responsible for the presence of Ce^{3+} in the fresh slurry. Both the creation of oxygen

vacancies on CeO_2 crystals and the diffusion of lattice oxygen atoms are relevant to the reduction of Ce^{4+} to Ce^{3+} [41,42]. Furthermore, as seen in Fig. 8(b) and (c), the N 1 s and B 1 s spectra of the fresh slurry both have just a single significant peak. More specifically, the N 1 s signal centered at 397.79 eV in Fig. 8(b) represents the N–B bonds of h-BN, and the peak at 190.21 eV in Fig. 8(c) is related to the B–N bonds of h-BN [43,44]. However, in addition to the binding energies of 529.17 eV for O^{2-} species in Ce^{4+} and 531.59 eV for O^{2-} species in Ce^{3+} , a new peak at 533.15 eV can be seen in the O 1 s spectra of the slurry after cyclic polishing (Fig. 8(d)). The binding energy of 533.15 eV is ascribed to O^{2-} in $\equiv\text{Si}-\text{O}-\text{Ce}=\$ bonding species [39,40], indicating that chemical reactions occurred between CeO_2 and FS during CMP. In addition, the corresponding peaks in the N 1 s and B 1 s spectra (Fig. 8(e) and (f)) of the slurry following cyclic polishing are essentially unchanged from those in Fig. 8(b) and (c).

During the CMP process, $\equiv\text{Si}-\text{O}-\text{Si}\equiv$ bonds were formed on the surface of FS due to its hydration. Moreover, some $\equiv\text{Si}-\text{O}-\text{Si}\equiv$ bonds were converted to $\text{Si}-\text{OH}$ silanol groups in the presence of water molecules. Based on the XPS spectra in Fig. 8, some of Ce^{4+} in the CeO_2 structure became Ce^{3+} species, and similarly, $=\text{Ce}-\text{OH}$ groups were formed on CeO_2 with the participation of water. In addition, due to the oxidability of Ce^{3+} , the Si–O bond was more susceptible to cleavage, and more $\equiv\text{Si}-\text{OH}$ groups were formed on the surface of FS [18]. In this instance, $=\text{Ce}-\text{OH}$ groups reacted with $\equiv\text{Si}-\text{OH}$ groups to form $\equiv\text{Si}-\text{O}-\text{Ce}=\$ bonds. Eqs. (2)–(4) can be used to describe the

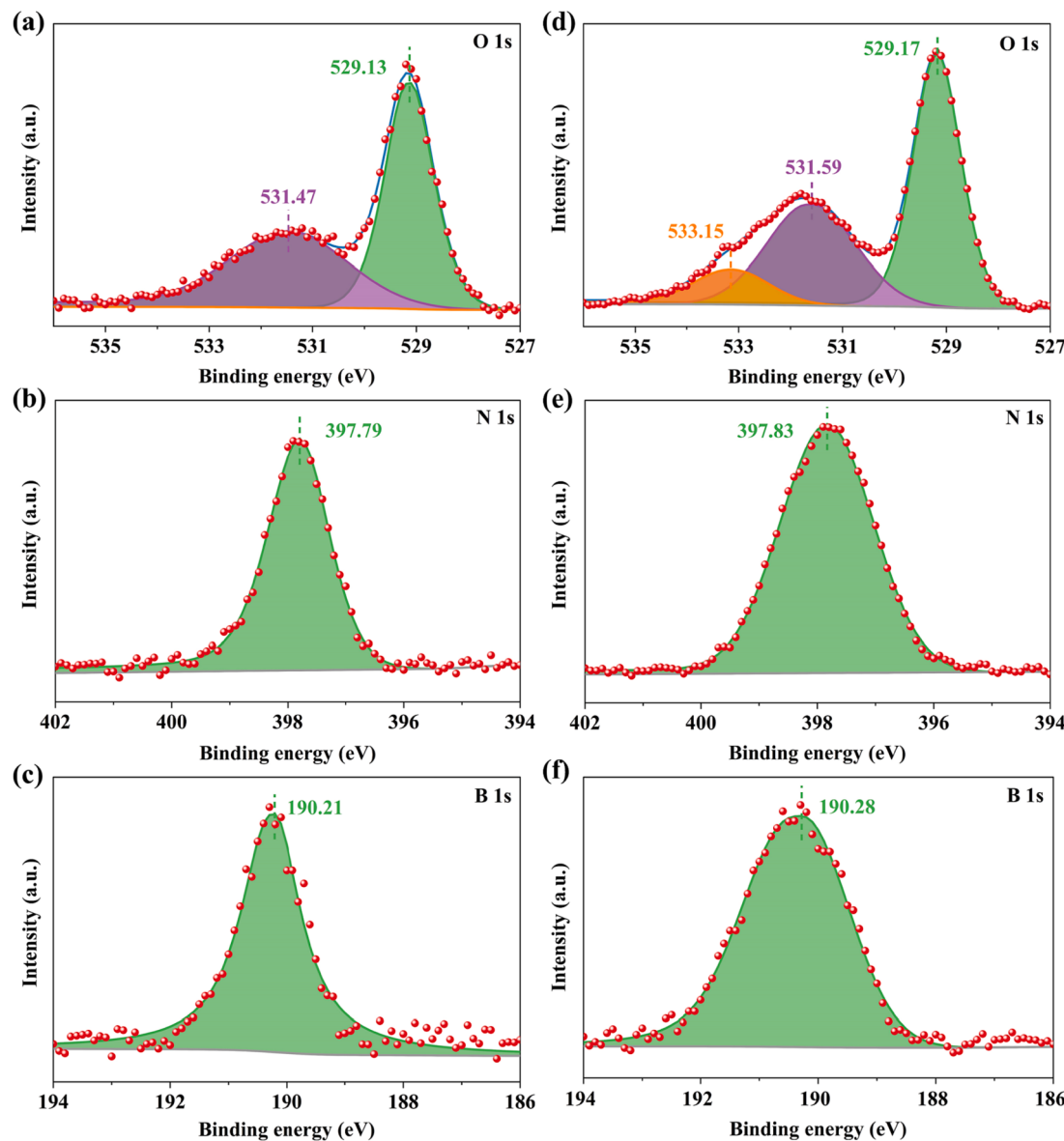
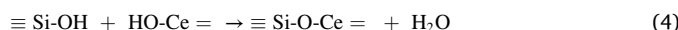
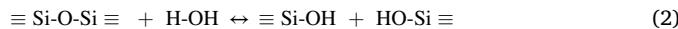


Fig. 8. XPS O 1 s, N 1 s, and B 1 s spectra of novel CMP slurry (a–c) before and (d–f) after polishing.

aforementioned analysis. Furthermore, since the B 1 s and N 1 s spectra of the slurry before and after cyclic polishing have almost identical peaks, h-BN in the novel CMP slurry was not involved in any chemical reactions throughout the CMP process could be explained.



The elemental composition and their valence changes for the FS before and after immersion in KOL solution were examined to further understand the role of KOL in CMP, and the related XPS spectra are shown in Fig. 9. In the O 1 s spectrum for the raw surface shown in Fig. 9(a), there are two main peaks at 532.60 and 531.93 eV, which are both identified as O²⁻ in SiO₂ [7,45]. The strong peak at 103.13 eV in Fig. 9(b) is ascribed to Si 2p in SiO₂ [45]. These findings show that SiO₂ was the only material present on the FS's raw surface. However, the O 1 s spectra in Fig. 9(c) of the FS treated with KOL solution are different from those in Fig. 9(a), with four primary peaks. Specifically, the binding energies at 533.42 and 531.07 eV are from O 1 s in O-C and O = C respectively

[46,47], which could be related to KOL. The binding energy at 532.67 eV is identified as the O 1 s signal from SiO₂ [45], and the binding energy at 532.08 eV is caused by the presence of SiO₃²⁻ [32]. In addition, the Si 2p spectrum in Fig. 9(d) with a peak centered at 103.22 eV is consistent with the Si 2p_{3/2} in SiO₂ [45]. The relatively weak peak at 102.60 eV is identified as the Si 2p_{1/2} in SiO₃²⁻ [32]. This indicates that a new species (SiO₃²⁻ species) was generated on the surface of FS after immersion in the KOL solution.

KOL is subject to hydrolysis in the presence of water. When KOL is hydrolyzed in water, it breaks down into its constituents: potassium cation (K⁺), oleate anion (C₁₇H₃₃COO⁻, OL⁻), and a water molecule (H₂O) [48,49]. In addition, KOL is also a potassium salt of oleic acid, and the oleate portion of its molecule has the potential to function as a weak base in an aqueous solution. In the presence of water, the carboxylate group (-COO⁻) in OL⁻ could accept a proton to form the carboxylic acid (-COOH, HOL) and hydroxide ion (OH⁻), which could raise the pH of the solution and make it more basic. In the alkaline solution, OH⁻ could react with FS to form a soluble salt, namely silicate, on the surface of FS. The above reaction mechanism for CMP can be described by the following equations:

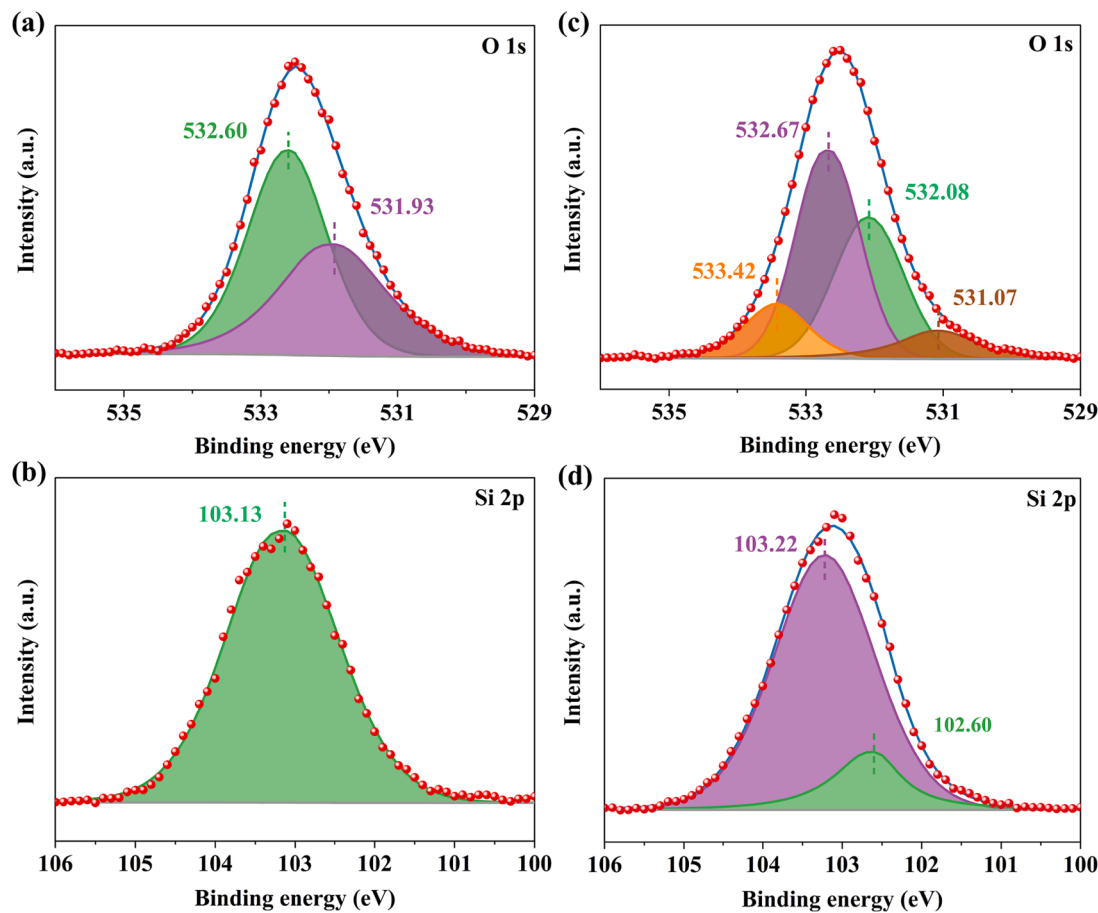
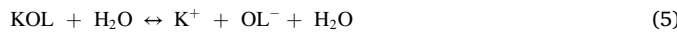


Fig. 9. XPS spectra of O 1s and Si 2p for FS (a, b) before and (c, d) after immersion in KOL solution.



The FTIR spectra were obtained and are shown in Fig. 10 to investigate the interactions between FS and the elements of the novel CMP slurry. Fig. 10(a) shows the FTIR spectrum of the FS sample utilized in this study in detail. There are three significant peaks centered at 1150.3, 791.1, and 467.7 cm^{-1} , which belong to the asymmetric stretching, symmetric stretching, and bending models of Si–O–Si, respectively

[50,51]. Besides, in the FTIR spectrum of KOL as illustrated in Fig. 10(b), the two distinct bands at 2920.1 and 2850.4 cm^{-1} correspond to the asymmetric and symmetric stretching vibrations of C–H bonds, respectively [52]. The bands at 1563.3 and 1415.6 cm^{-1} are both related to the carboxyl absorption bands, corresponding to the asymmetric and symmetric stretching vibrations of $-\text{COO}^-$ groups, respectively [53]. Furthermore, the last two bands at 1466.6 and 721.6 cm^{-1} in Fig. 10(b) are assigned to the scissoring vibration of the $-\text{CH}_2-$ groups and the rocking vibration of $-(\text{CH}_2)_n-$ ($n \geq 4$), respectively [54,55].

The bands near 2922.0, 2851.1, 1563.6, and 1416.3 cm^{-1} in Fig. 10(c) showed little difference from those in Fig. 10(b) when FS was treated with KOL solution. However, the bands at 1108.8, 783.5, and 470.1

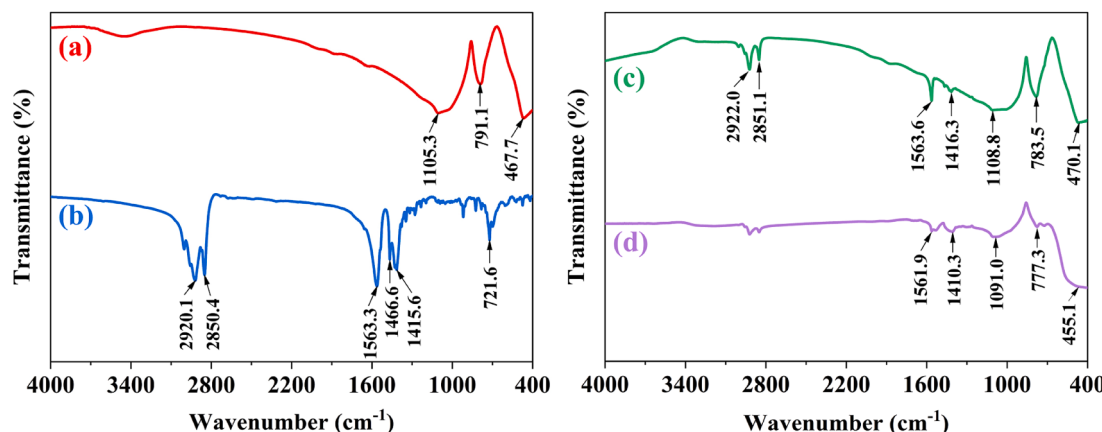


Fig. 10. FTIR spectra of (a) FS sample, (b) KOL, (c) FS treated with KOL, and (d) FS treated with slurry.

cm^{-1} (shifted from 1105.3, 791.1, and 467.7 cm^{-1} , respectively) demonstrate that the FS reacted with KOL solution, corresponding to Eqs. (5)–(7). Based on this, the typical absorption bands at 1105.3, 791.1, and 467.7 cm^{-1} were downshifted to 1091.0, 777.3, and 455.1 cm^{-1} , respectively, after treating FS with a mixed solution of KOL and CeO_2 , as shown in Fig. 10(d). The shifts of these bands could be related to the presence of $=\text{Ce}-\text{O}-\text{Si}\equiv$ bonds on the surface of FS due to the addition of CeO_2 [56]. These results are related to Eqs. (2)–(4). Besides, the bands related to carboxyl at 1563.3 and 1415.6 cm^{-1} were decreased to 1561.9 and 1410.3 cm^{-1} , respectively. This is probably due to the combination of Ce^{3+} with $-\text{COO}^-$, i.e., CeO_2 abrasives were modified by KOL, which could give the novel CMP slurry better fluidity, wettability, and dispersibility [57].

The sharp edges and corners of the abrasive made it simple to embed into the surface of FS while polishing it with conventional CeO_2 -based alkaline slurry, and the abrasives' primary behavior on FS was scratching. In this situation, the surface/subsurface would develop micro-cracks and other defects, resulting in the poor surface quality, as shown in Fig. 11(a). The superlubricity of the h-BN nanoflakes in the developed novel CMP slurry, however, caused most CeO_2 abrasives to switch from sliding to rolling instead of cutting the workpiece excessively. Finally, a relatively high surface quality was achieved after CMP, as depicted in Fig. 11(b).

A more thorough explanation of the CMP mechanism of FS is provided below based on the thorough investigation of the results above. During the CMP process, the hydration of FS and CeO_2 resulted in the formation of $\equiv\text{Si}-\text{OH}$ and $=\text{Ce}-\text{OH}$ groups. As a result of the strong interaction between the Ce and Si elements, $=\text{Ce}-\text{O}-\text{Si}\equiv$ bridging bridges were then produced, which had greater bonding energy than $\text{Si}-\text{O}-\text{Si}$ bonds. The original $\text{Si}-\text{O}$ bonds of FS were torn apart by the mechanical friction of CeO_2 abrasives, and finally, the removed material entered the slurry in the form of $=\text{Ce}-\text{O}-\text{Si}\equiv$, realizing the material removal of FS. In this procedure, h-BN served as a solid lubricant between the polishing pad, FS, and the abrasives, increasing the fluidity of abrasives and, more significantly, preventing the surface of the FS from excessive wear, producing a high-quality surface. Meanwhile, the hydroxyl ions (OH^-) were produced by the hydrolysis of KOL, which provided a suitable alkaline condition for polishing. A specific silicate formed on the surface of FS under these circumstances, which was afterward removed by abrasives. In addition, the combination of $-\text{COO}^-$ and Ce^{3+} enhanced the fluidity, wettability, and dispersibility of the slurry, which greatly increased the mechanical and chemical effects on the surface of FS, resulting in a high MRR. The result was the efficient

preparation of an ultra-smooth and low-damage surface due to the synergistic effect of chemical corrosion and mechanical wear.

4. Conclusions

In conclusion, a novel CMP slurry consisting of CeO_2 , h-BN, KOL, and DIW was developed for polishing FS. A super-smooth, super-low subsurface damage surface as well as an ultra-high MRR were concurrently attained after CMP by employing the novel CMP slurry. Comprehensive characterization and analysis revealed that the lubricity and flowability of the slurry were improved by the synergistic interaction between h-BN, a solid lubricant, and CeO_2 , a functional abrasive. The movement form of CeO_2 abrasives was modified from sliding to rolling with the aid of h-BN, preventing the excessive surface wear brought on by irregular CeO_2 abrasives. This significantly decreased the subsurface damage and substantially improved the surface roughness. The novel CMP slurry used KOL as a surfactant and pH regulator. In particular, KOL improved the activity of the slurry and offered a proper alkaline environment for polishing FS. In this instance, the polishing procedure effectively used more slurry, causing a thick modified layer of soluble silicate to build on the surface of the FS. The modified layer was then thoroughly removed by abrasives to achieve the material removal. In a nutshell, the synergistic effect of constituent parts of the novel CMP slurry helped to achieve high surface quality and MRR.

CRediT authorship contribution statement

Jie Liu: Investigation, Formal analysis, Data curation, Visualization. **Zhenyu Zhang:** Funding acquisition, Visualization, Project administration, Conceptualization, Methodology, Supervision. **Chunjing Shi:** Conceptualization, Methodology, Supervision, Investigation, Formal analysis, Data curation. **Zheng Ren:** Formal analysis, Data curation, Visualization. **Junyuan Feng:** Investigation, Methodology. **Hongxiu Zhou:** Investigation, Data curation. **Zhensong Liu:** Investigation, Methodology. **Fanning Meng:** Investigation, Visualization. **Shuming Zhao:** Investigation, Formal analysis.

Declaration of Competing Interest

The authors declare that they have no known competing financial interests or personal relationships that could have appeared to influence the work reported in this paper.

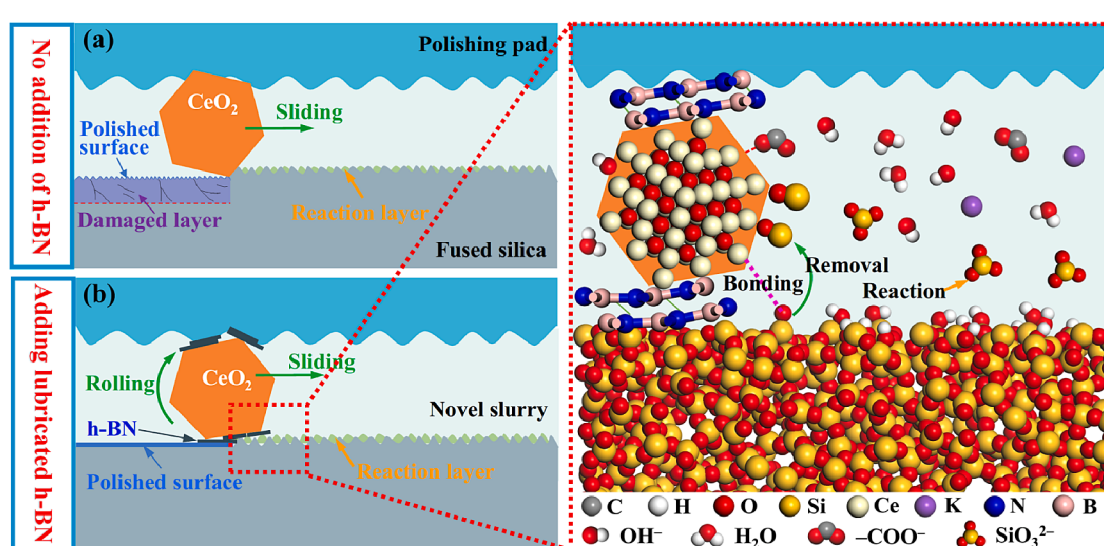


Fig. 11. Schematic diagram of CMP mechanism for FS with (a) conventional CMP slurry and (b) developed novel CMP slurry.

Data availability

The authors are unable or have chosen not to specify which data has been used.

Acknowledgments

The authors acknowledge the financial supports from the National Key Research and Development Program of China (2018YFA0703400), the Young Scientists Fund of the National Natural Science Foundation of China (52205447), the Key Field Science and Technology Projects of Yunnan Provincial Science and Technology Department (No. 202102AB080016), 2025 Major Program of Ningbo City for Innovation of Science and Technology (2020Z048), and the Changjiang Scholars Program of Chinese Ministry of Education.

References

- [1] F. Kotz, K. Arnold, W. Bauer, D. Schild, N. Keller, K. Sachsenheimer, T.M. Nargang, C. Richter, D. Helmer, B.E. Rapp, Three-dimensional printing of transparent fused silica glass, *Nature*. 544 (2017) 337–339, <https://doi.org/10.1038/nature22061>.
- [2] F. Kotz, A.S. Quick, P. Risch, T. Martin, T. Hoose, M. Thiel, D. Helmer, B.E. Rapp, Two-photon polymerization of nanocomposites for the fabrication of transparent fused silica glass microstructures, *Adv. Mater.* 33 (2021) 2006341, <https://doi.org/10.1002/adma.202006341>.
- [3] F. Kotz, N. Schneider, A. Striegel, A. Wolfschläger, N. Keller, M. Worgull, W. Bauer, D. Schild, M. Milich, C. Greiner, D. Helmer, B.E. Rapp, Glassomer—Processing fused silica glass like a polymer, *Adv. Mater.* 30 (2018) 1707100, <https://doi.org/10.1002/adma.201707100>.
- [4] J.T. Toombs, M. Luitz, C.C. Cook, S. Jenne, C.C. Li, B.E. Rapp, F. Kotz-Helmer, H. K. Taylor, Volumetric additive manufacturing of silica glass with microscale computed axial lithography, *Science*. 376 (2022) 308–312, <https://doi.org/10.1126/science.abm6459>.
- [5] G. Ren, H. Song, J. Dan, J. Li, P. Pan, Z. Yang, J. Xiao, J. Xu, Thermal analysis and machinability for laser-assisted machining of fused silica, *Int. J. Heat Mass Transfer*. 148 (2020), 119078, <https://doi.org/10.1016/j.ijheatmasstransfer.2019.119078>.
- [6] J. Cheng, Z. Yang, C. Wang, L. Zhao, M. Chen, J. Wang, Y. Li, Q. Xu, Z. Liu, H. Xu, Effect of scratches on the damage characteristics of fused silica optics under extremely-high impact load, *Int. J. Mech. Sci.* 219 (2022), 107099, <https://doi.org/10.1016/j.ijmecsci.2022.107099>.
- [7] G. Xu, Z. Zhang, F. Meng, L. Liu, D. Liu, C. Shi, X. Cui, J. Wang, W. Wen, Atomic-scale surface of fused silica induced by chemical mechanical polishing with controlled size spherical ceria abrasives, *J. Manuf. Processes*. 85 (2023) 783–792, <https://doi.org/10.1016/j.jmapro.2022.12.008>.
- [8] Z. Zhang, J. Liu, W. Hu, L. Zhang, W. Xie, L. Liao, Chemical mechanical polishing for sapphire wafers using a developed slurry, *J. Manuf. Processes*. 62 (2021) 762–771, <https://doi.org/10.1016/j.jmapro.2021.01.004>.
- [9] Z. Zhang, J. Cui, J. Zhang, D. Liu, Z. Yu, D. Guo, Environment friendly chemical mechanical polishing of copper, *Appl. Surf. Sci.* 467–468 (2019) 5–11, <https://doi.org/10.1016/j.apsusc.2018.10.133>.
- [10] J. Guo, X. Shi, C. Song, L. Niu, H. Cui, X. Guo, Z. Tong, N. Yu, Z. Jin, R. Kang, Theoretical and experimental investigation of chemical mechanical polishing of W-Ni-Fe alloy, *Int. J. Extrem. Manuf.* 3 (2021), 025103, <https://doi.org/10.1088/2631-7990/abefb8>.
- [11] X. Shi, G. Chen, L. Xu, C. Kang, G. Luo, H. Luo, Y. Zhou, M.S. Dargusch, G. Pan, Achieving ultralow surface roughness and high material removal rate in fused silica via a novel acid SiO₂ slurry and its chemical-mechanical polishing mechanism, *Appl. Surf. Sci.* 500 (2020), 144041, <https://doi.org/10.1016/j.apsusc.2019.144041>.
- [12] M.-Y. Tsai, W.-Z. Yang, Combined ultrasonic vibration and chemical mechanical polishing of copper substrates, *Int. J. Mach. Tools Manuf.* 53 (2012) 69–76, <https://doi.org/10.1016/j.ijmachtools.2011.09.009>.
- [13] Q. Mu, Z. Jin, X. Han, Y. Yan, Z. Zhang, P. Zhou, Effects of slurry pH on chemical and mechanical actions during chemical mechanical polishing of YAG, *Appl. Surf. Sci.* 563 (2021), 150359, <https://doi.org/10.1016/j.apsusc.2021.150359>.
- [14] Z. Zhang, L. Yu, W. Liu, Z. Song, Surface modification of ceria nanoparticles and their chemical mechanical polishing behavior on glass substrate, *Appl. Surf. Sci.* 256 (2010) 3856–3861, <https://doi.org/10.1016/j.apsusc.2010.01.040>.
- [15] K. Wakamatsu, S. Kurokawa, T. Toyama, T. Hayashi, CMP characteristics of quartz glass substrate by aggregated colloidal ceria slurry, *Precis. Eng.* 60 (2019) 458–464, <https://doi.org/10.1016/j.precisioneng.2019.06.014>.
- [16] N.-Y. Kim, G. Kim, H. Sun, U. Hwang, J. Kim, D. Kwak, I.-K. Park, T. Kim, J. Suhr, J.-D. Nam, A nanoclustered ceria abrasives with low crystallinity and high Ce³⁺/Ce⁴⁺ ratio for scratch reduction and high oxide removal rates in the chemical mechanical planarization, *J. Mater. Sci.* 57 (2022) 12318–12328, <https://doi.org/10.1007/s10853-022-07338-x>.
- [17] P. Janoš, J. Ederer, V. Pilařová, J. Henych, J. Tolasz, D. Milde, T. Opletal, Chemical mechanical glass polishing with cerium oxide: Effect of selected physico-chemical characteristics on polishing efficiency, *Wear*. 362–363 (2016) 114–120, <https://doi.org/10.1016/j.wear.2016.05.020>.
- [18] Z. Wu, Z. Zhang, Y. Jia, F. Teng, G. Li, F. Wang, Y. Jin, Fused silica with sub-angstrom roughness and minimal surface defects polished by ultrafine nano-CeO₂, *J. Am. Ceram. Soc.* 106 (2023) 1766–1777, <https://doi.org/10.1111/jace.18884>.
- [19] K. Kim, D.K. Yi, U. Paik, Increase in Ce³⁺ concentration of ceria nanoparticles for high removal rate of SiO₂ in chemical mechanical planarization, *ECS J. Solid State Sci. Technol.* 6 (2017) P681–P685, <https://doi.org/10.1149/2.0371709jss>.
- [20] J. Seo, K. Kim, H. Kang, S.V. Babu, Perspective—Recent advances and thoughts on ceria particle applications in chemical mechanical planarization, *ECS J. Solid State Sci. Technol.* 11 (2022), 084003, <https://doi.org/10.1149/2162-8777/ac8310>.
- [21] J. Ma, N. Xu, Y. Luo, Y. Lin, Y. Pu, Enhancing the polishing efficiency of CeO₂ abrasives on the SiO₂ substrates by improving the Ce³⁺ concentration on their surface, *ACS Appl. Electron. Mater.* 5 (2023) 526–536, <https://doi.org/10.1021/acsaelm.2c01553>.
- [22] H. Xiao, S. Liu, 2D nanomaterials as lubricant additive: A review, *Mater. Design*. 135 (2017) 319–332, <https://doi.org/10.1016/j.matdes.2017.09.029>.
- [23] J.C. Spear, B.W. Ewers, J.D. Batteas, 2D-nanomaterials for controlling friction and wear at interfaces, *Nano Today*. 10 (2015) 301–314, <https://doi.org/10.1016/j.nantod.2015.04.003>.
- [24] M. Marian, G.C. Song, B. Wang, V.M. Fuenzalida, S. Krauß, B. Merle, S. Tremmel, S. Wartzack, J. Yu, A. Rosenkranz, Effective usage of 2D MXene nanosheets as solid lubricant – Influence of contact pressure and relative humidity, *Appl. Surf. Sci.* 531 (2020), 147311, <https://doi.org/10.1016/j.apsusc.2020.147311>.
- [25] J. Chen, J. Chen, S. Wang, Q. Sun, J. Cheng, Y. Yu, J. Yang, Tribological properties of h-BN matrix solid-lubricating composites under elevated temperatures, *Tribol. Int.* 148 (2020), 106333, <https://doi.org/10.1016/j.triboint.2020.106333>.
- [26] C. Xiao, F.-C. Hsia, A. Sutton-Cook, B. Weber, S. Franklin, Polishing of polycrystalline diamond using synergies between chemical and mechanical inputs: A review of mechanisms and processes, *Carbon*. 196 (2022) 29–48, <https://doi.org/10.1016/j.carbon.2022.04.028>.
- [27] Y. Guo, W. Song, L. Guo, X. Li, W. He, X. Yan, D.B. Dingwell, H. Guo, Molten-volcanic-ash-phobic thermal barrier coating based on biomimetic structure, *Adv. Sci.* 10 (2023) 2205156, <https://doi.org/10.1002/advs.202205156>.
- [28] T. Huhtamäki, X. Tian, J.T. Korhonen, R.H.A. Ras, Surface-wetting characterization using contact-angle measurements, *Nat. Protoc.* 13 (2018) 1521–1538, <https://doi.org/10.1038/s41596-018-0003-z>.
- [29] J. Zheng, Y. Lyu, M. Qiao, R. Wang, Y. Zhou, H. Li, C. Chen, Y. Li, H. Zhou, S. P. Jiang, S. Wang, Photoelectrochemical synthesis of ammonia on the aerophilic-hydrophilic heterostructure with 37.8% efficiency, *Chem.* 5 (2019) 617–633, <https://doi.org/10.1016/j.chempr.2018.12.003>.
- [30] X. Sun, Q. Zhu, J. Hu, X. Kang, J. Ma, H. Liu, B. Han, N, N-Dimethylation of nitrobenzenes with C₆₀ and water by electrocatalysis, *Chem. Sci.* 8 (2017) 5669–5674, <https://doi.org/10.1039/C7SC01058C>.
- [31] D. Liu, Z. Zhang, J. Feng, Z. Yu, F. Meng, C. Shi, G. Xu, S. Shi, W. Liu, Environment-friendly chemical mechanical polishing for copper with atomic surface confirmed by transmission electron microscopy, *Colloids Surf. A*. 656 (2023), 130500, <https://doi.org/10.1016/j.colsurfa.2022.130500>.
- [32] Z. Zhao, Z. Zhang, C. Shi, J. Feng, X. Zhuang, L. Li, F. Meng, H. Li, Z. Xue, D. Liu, Dispersion and polishing mechanism of a novel CeO₂-LaOF-based chemical mechanical polishing slurry for quartz glass, *Materials*. 16 (2023) 1148, <https://doi.org/10.3390/ma16031148>.
- [33] J. Wang, F. Ma, W. Liang, M. Sun, Electrical properties and applications of graphene, hexagonal boron nitride (h-BN), and graphene/h-BN heterostructures, *Mater. Today Phys.* 2 (2017) 6–34, <https://doi.org/10.1016/j.mtphys.2017.07.001>.
- [34] D. Steiner, F. Mittendorfer, E. Bertel, Quasiliquid layer promotes hexagonal boron nitride (h-BN) single-domain growth: h-BN on Pt(110), *ACS Nano*. 13 (2019) 7083–7090, <https://doi.org/10.1021/acsnano.9b02377>.
- [35] S. Xing, G. Zhao, Y. Xu, J. Wang, X. Li, W. Yang, G. Liu, J. Yang, Determination of band alignment in two-dimensional h-BN/WS₂ van der waals heterojunction by X-ray photoelectron spectroscopy, *J. Alloys Compd.* 854 (2021), 157301, <https://doi.org/10.1016/j.jallcom.2020.157301>.
- [36] J. Tian, H. Liu, J. Cheng, M. Chen, B. Qin, Improving the small ball-end magnetorheological polishing efficiency of fused silica workpiece by the promoting effect of water-bath heating and sodium hydroxide addition on polishing velocity and chemical reaction, *Int. J. Adv. Manuf. Technol.* 123 (2022) 645–656, <https://doi.org/10.1007/s00170-022-10180-9>.
- [37] N. Xu, J. Ma, Q. Liu, Y. Luo, Y. Pu, Preparation of CeO₂ abrasives by reducing atmosphere-assisted molten salt method for enhancing their chemical mechanical polishing performance on SiO₂ substrates, *J. Rare Earths*. (2022) S100207212200312X. 10.1016/j.jre.2022.10.011.
- [38] Y. Zhou, H. Luo, G. Luo, C. Kang, G. Chen, G. Pan, Characteristics of slurry recycling in chemical mechanical polishing (CMP) of fused silica (FS), *ECS J. Solid State Sci. Technol.* 8 (2019) P196–P201, <https://doi.org/10.1149/2.0121903jss>.
- [39] Y. Zhou, H. Luo, G. Luo, G. Chen, C. Kang, G. Pan, Chemical mechanical polishing (CMP) of fused silica (FS) using ceria slurry recycling, *ECS J. Solid State Sci. Technol.* 9 (2020), 044002, <https://doi.org/10.1149/2162-8777/ab8391>.
- [40] C. Kang, B. Gao, D. Guo, H. Luo, G. Pan, The cycle characteristics of slurries in chemical mechanical polishing (CMP) of fused silica, *ChemistrySelect*. 5 (2020) 9350–9356, <https://doi.org/10.1002/slct.202000926>.
- [41] N.V. Skorodumova, S.I. Simak, B.I. Lundqvist, I.A. Abrikosov, B. Johansson, Quantum origin of the oxygen storage capability of ceria, *Phys. Rev. Lett.* 89 (2002), 166601, <https://doi.org/10.1103/PhysRevLett.89.166601>.
- [42] L. Zhu, X. Jin, Y. Zhang, S. Du, L. Liu, T. Rajh, Z. Xu, W. Wang, X. Bai, J. Wen, L. Wang, Visualizing anisotropic oxygen diffusion in ceria under activated conditions, *Phys. Rev. Lett.* 124 (2020), 056002, <https://doi.org/10.1103/PhysRevLett.124.056002>.

- [43] J. Hadid, I. Colambo, C. Boyaval, N. Nuns, P. Dudin, J. Avila, X. Wallart, D. Vignaud, Molecular beam epitaxial growth of hexagonal boron nitride on Ni foils, *2D Mater.* 8 (2021), 045007, <https://doi.org/10.1088/2053-1583/ac1502>.
- [44] K.P. Sharma, S. Sharma, A. Khaniya Sharma, B. Paudel Jaisi, G. Kalita, M. Tanemura, Edge controlled growth of hexagonal boron nitride crystals on copper foil by atmospheric pressure chemical vapor deposition, *CrystEngComm.* 20 (2018) 550–555, <https://doi.org/10.1039/C7CE01846K>.
- [45] M. Green, Z. Liu, P. Xiang, Y. Liu, M. Zhou, X. Tan, F. Huang, L. Liu, X. Chen, Doped, conductive SiO_2 nanoparticles for large microwave absorption, *Light: Sci. Appl.* 7 (2018) 87, <https://doi.org/10.1038/s41377-018-0088-8>.
- [46] C.I. Ogbu, X. Feng, S.N. Dada, G.W. Bishop, Screen-printed soft-nitrided carbon electrodes for detection of hydrogen peroxide, *Sens.* 19 (2019) 3741, <https://doi.org/10.3390/s19173741>.
- [47] Y. Shi, D.J. Noelle, M. Wang, A.V. Le, H. Yoon, M. Zhang, Y.S. Meng, Y. Qiao, Role of amines in thermal-runaway-mitigating lithium-ion battery, *ACS Appl. Mater. Interfaces.* 8 (2016) 30956–30963, <https://doi.org/10.1021/acsami.6b10501>.
- [48] L. Hu, G. Pan, H. Wang, X. Zhang, Z. Wang, T. Zhu, The synergy and DFT study of TT-LYK and potassium oleate on chemical mechanical polishing of cobalt in alkaline medium, *Mater. Chem. Phys.* 256 (2020), 123672, <https://doi.org/10.1016/j.matchemphys.2020.123672>.
- [49] S. Bai, J. Li, Y. Bi, J. Yuan, S. Wen, Z. Ding, Adsorption of sodium oleate at the microfine hematite/aqueous solution interface and its consequences for flotation, *Int. J. Min. Sci. Technol.* 33 (2023) 105–113, <https://doi.org/10.1016/j.ijmst.2022.09.012>.
- [50] A. Elimbi, S. Njouonkou, J. Ndi Nsami, P.D. Belibi Belibi, J. Ketcha Mbadkam, Adsorption test of methylene blue onto porous powdered ceramics obtained from mixtures of kaolin–bauxite and kaolin–oyster shell, *Int. J. Environ. Sci. Technol.* 16 (2019) 1337–1350, <https://doi.org/10.1007/s13762-018-1754-3>.
- [51] N. Hosseini Mohtasham, M. Gholizadeh, Nano silica extracted from horsetail plant as a natural silica support for the synthesis of $\text{H}_3\text{PW}_{12}\text{O}_{40}$ immobilized on aminated magnetic nanoparticles ($\text{Fe}_3\text{O}_4@\text{SiO}_2\text{-EP-NH-HPA}$): a novel and efficient heterogeneous nanocatalyst for the green one-pot synthesis of pyrano[2,3-c]pyrazole derivatives, *Res. Chem. Intermed.* 46 (2020) 3037–3066, <https://doi.org/10.1007/s11164-020-04133-8>.
- [52] M. Ammar, S.A. El-Halim, H. Sharada, M. Fadel, A. Yehia, Study on the interactions of two models of enzymes as eco-friendly depressants in flotation separation of apatite from hematite, *Appl. Surf. Sci.* 601 (2022), 154223, <https://doi.org/10.1016/j.apsusc.2022.154223>.
- [53] R. Popuri, H. Amanapu, C.K. Ranaweera, N.K. Baradanahalli, S.V. Babu, Potassium oleate as a dissolution and corrosion inhibitor during chemical mechanical planarization of chemical vapor deposited co films for interconnect applications, *ECS J. Solid State Sci. Technol.* 6 (2017) P845–P852, <https://doi.org/10.1149/2.0251712jss>.
- [54] J. Liu, Q. Zhang, F. Ma, S. Zhang, Q. Zhou, A. Huang, Three-step identification of infrared spectra of similar tree species to *Pterocarpus santalinus* covered with beeswax, *J. Mol. Struct.* 1218 (2020), 128484, <https://doi.org/10.1016/j.molstruc.2020.128484>.
- [55] M. Wang, G. Huang, G. Zhang, Y. Chen, D. Liu, C. Li, Selective flotation separation of fluorite from calcite by application of flaxseed gum as depressant, *Miner. Eng.* 168 (2021), 106938, <https://doi.org/10.1016/j.mineng.2021.106938>.
- [56] T. Hoshino, Y. Kurata, Y. Terasaki, K. Susa, Mechanism of polishing of SiO_2 films by CeO_2 particles, *J. Non-Cryst. Solids.* 283 (2001) 129–136, [https://doi.org/10.1016/S0022-3093\(01\)00364-7](https://doi.org/10.1016/S0022-3093(01)00364-7).
- [57] M. Wang, X. Zeng, Z. Shen, J. Chen, Surface modification of CeO_2 nanoparticles and their dispersion properties in aqueous media, *J. Beijing Univ. Chem. Technol. (Nat. Sci. Ed.)*, 38 (2011) 6–11. 10.13543/j.cnki.bhxzr.2011.04.024.